NANO MICRO
small

Supporting Information

For *Small*, DOI: 10.1002/smll.201002186

Hybrid Top-down and Bottom-up Fabrication Approach for Wafer-scale Plasmonic Nano-Platforms

By Anuj Dhawan, Yan Du, Dale Batchelor, Hsin-Neng Wang, Donovon Leonard, Veena Misra, Mehmet Ozturk, Michael Gerhold, and Tuan Vo-Dinh*

NANO MICRO small

Supporting Information

Section S1. Relationship between SERS EM Enhancement and E-Field Enhancement

There are two main sources of electromagnetic (EM) enhancement of SERS[S1-S2] – The first source of enhancement is due to excitation of surface plasmons (SPs).[S3-S4] Such a plasmonic EM enhancement in the vicinity of SERS substrates containing Raman-active molecules leads to an increase in Raman scattering intensity, which is proportional to square of applied field at the molecule. Due to the additional enhancement of Raman signal of analyte molecules, the total EM enhancement factor is proportional to the fourth power of the electric field around the nanostructures. Relationship between SERS signal intensity and localized electric field in the vicinity of metallic nanostructures has been described as the product of average local field intensity (E_{loc}) at the surface of SERS substrate:[S1-S2]

$$\mathrm{CEME} = \left\langle \left| \frac{E_{loc}(\omega_L)}{E_{inc}(\omega_{L,}\Omega_L)} \right|^2 \right\rangle \left\langle \left| \frac{E_{loc}(\omega_S)}{E_{inc}(\omega_{S,}\Omega_S)} \right|^2 \right\rangle \qquad (1)$$

where frequency and direction of the incident radiation are ω_L and Ω_L respectively, E_{inc} the incident electric field strength, ω_S is the Stokes frequency of emitted Raman signal, which is emitted in the direction Ω_S.

Section S2. Plasmonic Enhancement of EM Fields in between Metallic Nanowires

S2.1. Theoretical background for plasmonic enhancement of EM Fields in one dimensional metallic gratings

Wirgin et al.[S5] derived mathematical relationships between the electric and magnetic fields in between rectangular grooves in zero-order silver gratings and demonstrated a substantial increase in the electric field intensity inside the grooves as the spacing between the metallic gratings decreased. Tan et al.[S6] and Garcia Vidal et al.[S7] explained the phenomenon of coupling of p-polarized incident radiation to surface plasmon polariton (SPP) modes in short-pitch metallic gratings. The narrow width of the grooves leads to strong coupling

between surface charges on opposing walls of an individual grating groove, thereby leading to formation of standing SPP modes localized inside the groove. The coupling between the SPP modes inside the individual grooves increases with decreasing groove width. Each SPP standing mode in the individual grooves couples to the corresponding mode in the neighboring grooves leading to formation of very flat SPP bands. Due to the generation of a series of standing SPP modes inside each groove, the dispersion relation (ω-kx relationship) of the grating has multiple points of intersection with the light line (dispersion relation of the incident radiation, kx = ω/c) indicating coupling of multiple wavelengths to the SPP modes in the individual grooves in the grating.

Garcıa-Vidal et al.[S7] have described that for p-polarized light (having wavelength λ, $k_0 = 2\pi/\lambda$) being incident normally on a metallic reflection grating - a metallic film having periodic rectangular grooves with a periodicity '*p*' and λ> *p* and the length of the grooved surface being infinitely long in one direction - the amplitude of the electric field inside the grooves (E_{groove}) can be expressed in terms of the amplitude of the incident electric field ($E_{incident}$) as given by equation (2):

$$E_{groove} \approx \frac{p}{w} \frac{e^{ik_0 h}}{\sin(k_0 h)} E_{incident} \qquad (2)$$

where '*w*' and '*h*' are the width and height of the rectangular grooves, respectively. In the case of cavity resonances (λ>>*h*), $\sin(k_0 h) = 1$ and enhancement of the electric-field intensity inside the grooves as a function of the incident field is proportional to $(p/w)^2$. Although the metal-coated (plasmonics-active metals such as gold and silver) diamond-shaped nanowires (DNWs) have a cross-sectional geometry different from rectangular metallic nano-gratings, the theoretical description by Garcıa-Vidal et al.[S7] qualitatively explains the high EM fields (and therefore the SERS signals from molecules lying in the nano-scale gaps) from the nano-scale gaps between the metallic lines of the nano-gratings. The FDTD calculations provided

below provide further insight into the EM field enhancement in the nano-scale gaps in the DNWs, as well as an increase in the EM field enhancement as the smallest gap between the nanowires is reduced.

S2.2. Finite Difference Time Domain (FDTD) calculations

We performed numerical calculations using the Finite Difference Time Domain (FDTD) method to determine the electric field enhancement in the nano-scale gaps in the DNW substrates. In the FDTD method, the time-dependent Maxwell's equations are discretized using central-difference approximations to the space and time partial derivatives. In our calculations, gold-coated diamond-shaped silicon nanowires were simulated as shown in Figure 3a of the main paper. In the FDTD calculations, a continuous plane wave, with polarization of the electric field being in the x-direction, was incident on the gold nanowire structures with the wave propagating in the z direction and the enhancement in the electric field as a function of the incident field (which was normalized to have a value of 1) determined. To avoid simulating structures that could not be developed in practice, the tips of the diamond-shaped nanowire structures had a radius of curvature of at least 25 nm. Two dimensional Finite Difference Time Domain (FDTD)[S8] calculations of electric fields in the spacings between the DNWs were carried out using FDTD software called Fullwave 6.0. This software enables FDTD analysis of the metallic media to include Debye or Lorentz models of dispersion relations of the dielectric constants of the metals. In the simulations, we use the following dispersion model (an extended Debye model) for determining the dielectric constant for gold and silver:

$$\varepsilon(\omega) = 1 + \sum_{k=1}^{6} \frac{\Delta\varepsilon_k}{a_k\omega^2 \quad ib_k\omega + c_k} \qquad (3)$$

where $\Delta\varepsilon_k$, a_k, b_k *and* c_k are constants.[S9-S10] The time steps (Δt) employed in these simulations were selected to be small enough such that the Courant stability criterion[S8] described by

equation (4) was satisfied for the different grid sizes (Δx, Δy, and Δz) employed, where c is the speed of light:

$$\Delta t < \frac{1}{c\sqrt{\frac{1}{(\Delta x)^2}+\frac{1}{(\Delta y)^2}+\frac{1}{(\Delta z)^2}}} \quad (4)$$

In the FDTD simulations, perfectly matched layers (PML) having a reflection coefficient $\Gamma=10^{-8}$ and a grid size of 1nm were employed. A simulation time step $c\Delta t$ = 1nm ('c' being the speed of light) was chosen to satisfy the Courant stability criterion at this resolution, and each simulation was run for long enough time duration to ensure that the system reached a steady state. The FDTD simulations were performed by employing a continuous plane wave excitation that is incident normally on the nanowire structures (for both 633 nm and 785 nm wavelengths of the incident radiation).

Section S3. Fabrication of Diamond-Shaped Nanowire Structures

Previously researchers have described the development of Si, Ge, and $Si_{1-x}Ge_x$ nanowires using the vapor-liquid-solid[11] and vapor-solid-solid growth mechanisms[12]. In order to develop the Diamond-shaped nanowire structures, we employed a combination of deep UV lithography (to develop silicon nanostructures) and controlled epitaxial growth of silicon germanium on certain facets of the silicon nanostructures. This led to the development of diamond shaped nanowires with controllable gaps between neighboring nanowire structures on the scale of the entire wafer. The different fabrication steps involved in the development of gold-coated diamond-shaped nanowires are depicted in the schematic shown in Figure S1.

The first fabrication step involved the development of silicon nanowires on 6-inch silicon as well as silicon-on-insulator (SOI) wafers. In order to develop the silicon nanowires, deep UV lithography (193-nm UV lithography using an ASML 5500/950B Scanner) was employed in conjunction with reactive ion etching. Silicon nanowires of different sizes and spacings

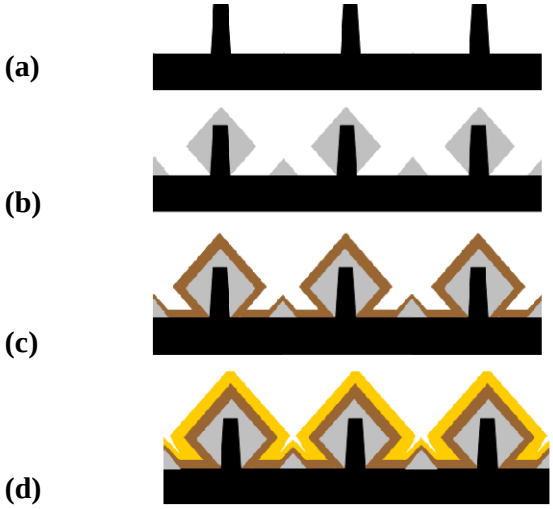

Figure S1. A schematic showing the development of gold-coated diamond-shaped nanowires. The first step (a) involved development of silicon nanowires (shown in black color) by using deep UV lithography. The second step (b) involved the development of the diamond-shaped geometry of these nanowires due to growth of silicon germanium (in grey color) on the underlying silicon nanowires (in black) using Rapid Thermal Chemical Vapor deposition (RTCVD). The diamond-shaped nanowires were coated (this is an optional step) with a spacer layer - of hafnium oxide or platinum (depicted in brown color in step (c) of Figure S1) using atomic layer deposition (ALD) - to controllably reduce the spacing between the nanowires and to change the size of the nanowires. Finally gold (in yellow) was evaporated on the underlying layers to form gold-coated diamond-shaped nanowires on a wafer scale.

between the nanowires (varying between 100 nm to 10 microns) were developed over the entire 6-inch wafer.

To develop DNW structures, silicon germanium i. e. $Si_{1-x}Ge_x$ epitaxial films were grown on the silicon nanowires and then overcoated with a thin layer of silver or gold (See Figures 2a-d of the main paper). Rapid thermal chemical vapor deposition (RTCVD) at high vacuum (10^{-9} Torr) was employed for the growth of silicon germanium. Disilane (Si_2H_6), Germane (GeH_4), and hydrogen gases were flown into the CVD chamber during the growth process at

flow rates 15 sccm, 45 sccm, and 400 sccm, respectively, such that the proportion of germanium in the silicon germanium layer was 28%. The (111) facet growth was primarily observed in the silicon germanium epitaxial films. A $Si_{1-x}Ge_x$ epitaxial film growth rate of 40 nm/min was observed. During the epitaxial growth of silicon germanium on silicon (100) substrates with patterns aligned along [100], (111) and (311) facet growths were typically observed. At the growth temperature of 550 ^{o} C, (111) facet growth was dominantly observed (See Figures 2a-d of the main paper).

The third fabrication step involved atomic layer deposition (ALD) of hafnium oxide or platinum to form a conformal layer designed to precisely control the gap between the nanowires and the nanowire width in a reproducible manner (See Figure 2e of the main paper). ALD was employed for depositing platinum – which could act as either a conformal spacer layer or as the metal layer for the SERS substrate or both - on the diamond-shaped nanowires. Figure 2e of the main paper shows a transmission electron microscopy (TEM) cross-sectional image of a thin film of platinum deposited by employing ALD on the surface of diamond-shaped nanowire structures (formed by epitaxial growth of silicon germanium on silicon nanowires formed on SOI substrates). The platinum deposition on $Si_{1-x}Ge_x$ nanowires was carried out at 300 degrees C, the deposition rate of the platinum film being approximately 0.06 nm/cycle. The processing parameters for each cycle included 1 second platinum precursor time, followed by a nitrogen purging time of 3 seconds, oxygen flow time of 0.25 seconds, and a final nitrogen purge of 3 seconds. The ALD of hafnium oxide on the silicon germanium nanowires was carried out at 200 degrees C at a rate of 0.075 nm/cycle.

The final fabrication process in the development of the DNW SERS substrates involves over coating of the diamond shaped nanowire structures with plasmonics-active materials such as gold or silver (20-100 nm thick films are deposited) using sputtering or electron beam evaporation. In the case of electron beam (or E-beam) evaporation of gold, deposition rates

between 0.05 nm s^{-1} and 0.2 nm s^{-1} were employed while in the case of sputtering of gold, deposition rate was ~ 0.5 nm s^{-1}.

Section S4. Fabrication of Two-Dimensional Nanowire Arrays

To fabricate two-dimensional nanowire arrays (Figures S2a-b), we incorporated another step following the development of silicon nanowires using deep UV lithography, in which parts of the silicon nanowires were periodically covered by SiO_2 using a second masking process and a deep UV lithography step to create SiO_2 lines running in the direction perpendicular to the silicon nanowires. When the silicon germanium growth was carried out on this structure, growth of silicon germanium to form the diamond-shaped structure took place only in regions where silicon was not covered by the SiO_2 lines as the SiO_2 layer prevented the formation of diamond-shaped structures. Figure S2a (right) shows a two dimensional array of diamond-shaped silicon germanium nanowires that are periodically spaced with nano-scale gaps or regions where the nanowires end along the length of the nanowires. These regions correspond to the regions where the SiO_2 lines were deposited. Figure S2b shows a gold-coated two-dimensional array of DNW structures, each DNW unit being ~150 nm wide and 180 nm long with ~ 40 nm gap between two successive nanowires along the length of the nanowires. Between two parallel DNWs in the two-dimensional array of nanowires, there are small triangular sections and the nanoscale gap between the gold film on the diamond-shaped nanowires and these triangular sections is less than 10 nm. The ability to fabricate gold nanowires of different lengths with varying spacings between adjacent nanowires along the long or short axes of the nanowires (Figure S2b and Figure S2c) enables tuning the localized surface plasmon resonance wavelength of the nanostructures with the incident light wavelength when these nanowires are over-coated with a coinage noble metals (e.g., gold, silver, or copper). Moreover, it provides a means of developing nanoscale gaps between

metallic nanostructures in two dimensions – i.e. along the length or width of the nanowires as depicted in Figure S2b.

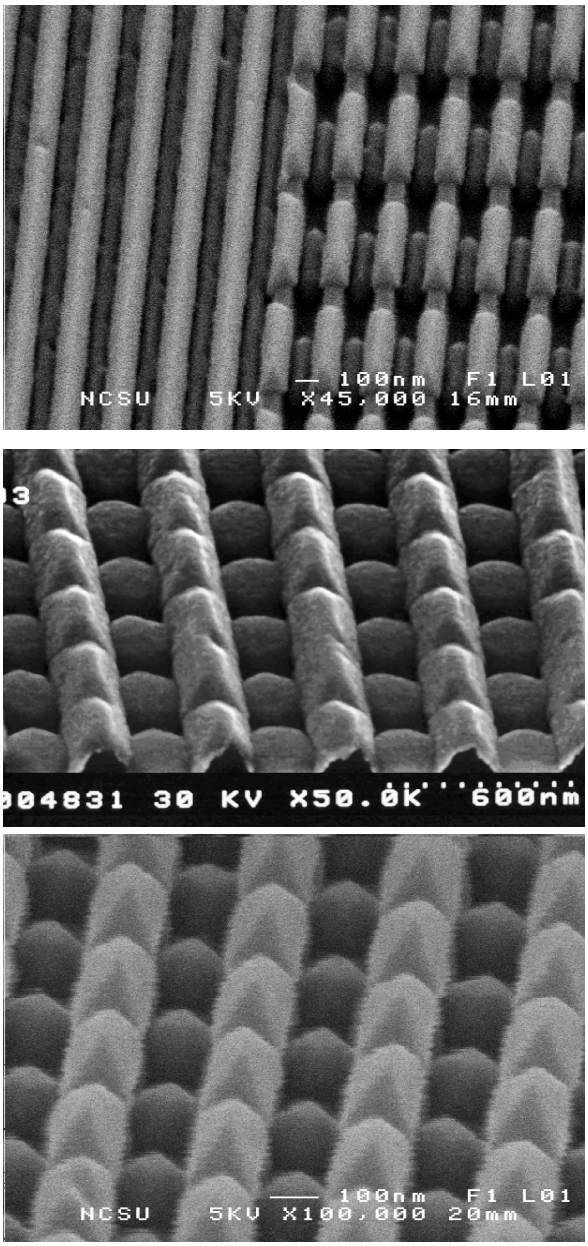

Figure S2. (a) SEM image of uncoated epitaxially grown silicon germanium ($Si_{1-x}Ge_x$) nanowires – one dimensional nanowire array on the left and two dimensional array on the right. (b)-(c) Two-dimensional silicon germanium diamond-shaped nanowires (DNWs) (b) with gold coating and (c) without gold coating.

Section S5. Application of the Nanowire Chips for Detection of Anthrax Marker

Figure 3i (of the main paper) shows the application of DNW SERS substrates for detection of dipicolinic acid (DPA), a biomarker for spores of bacteria such as Anthrax (*Bacillus anthracis*). SERS spectrum of DPA exhibited strong Raman spectral bands at 998 cm^{-1} and 1569 cm^{-1}, corresponding to symmetric ring breathing and ring stretching band, respectively. Other SERS bands were at 1080 cm^{-1}, 1185 cm^{-1}, 1385 cm^{-1} and 1428 cm^{-1}, corresponding to trigonal ring breathing mode, C-H bending mode, the C-O stretching mode, and C-C ring stretching mode, respectively.

Section S6. Printing of Molecules on the DNW Chips

Figure S3 shows patterns of DNA molecules printed on the gold coated DNWs using a Nano eNabler molecular printer. A molecular printer, called the Nano eNabler, can dispense very small volumes of liquids (and 1-30 μm sample droplets) such as proteins [S13] and oligonucleotides at defined positions to create patterns of spots or lines with high spatial accuracy. The Nano eNabler consists of a compact precision motion control platform mated to

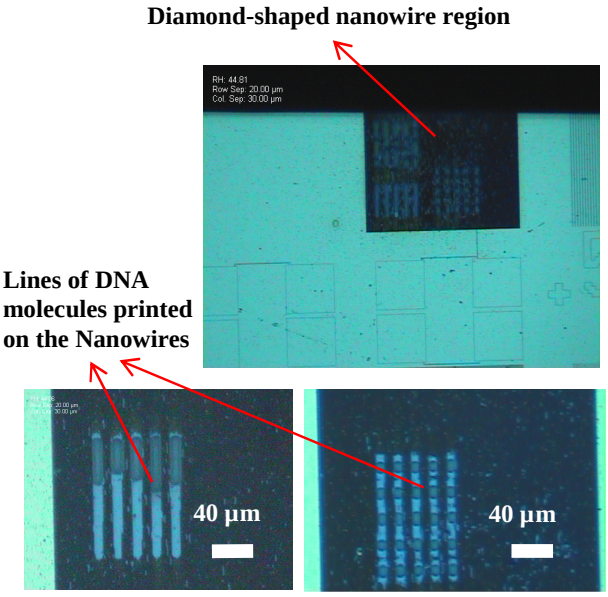

Figure S3. A picture showing lines of DNA molecules printed on a linear array of gold coated diamond-shaped nanowires (present on a nanowire chip) by employing a molecular printer.

a microfabricated surface patterning tool with integrated microfluidics. A Surface patterning tool is a microcantilever-based micro-fluidic handling device and contains microcantilever print heads for printing of multiple molecular species as well as a microfluidic network that transports fluid samples (the DNA molecules and other analytes to be printed) from macroscale reservoirs located on the surface patterning tool substrate through microchannels to the distal end of the cantilever.

[S1] A. Otto, I. Mrozek, H. Grabhorn, W. Akemann, *J. Phys: Condensed Matter* **1992**, *4*, 1143.

[S2] M. Moskovits, *Rev. Mod. Phys.* **1985**, *57*, 783.

[S3] R. K. Chang, T. E. Furtak, Eds. *Surface-Enhanced Raman Scattering*, Plenum, New York **1982**.

[S4] M. Fleischmann, P.J. Hendra, A.J. McQuillan, *Chem. Phys. Lett.* **1974**, *26*, 163.

[S5] A. Wirgin, T. Lopez-Rios, *Optics Comm.* **1984**, *48*, 416.

[S6] W. C. Tan, T. W. Preist, J. R. Sambles, N. P. Wanstall, *Phys. Rev. B* **1999**, *59*, 12661.

[S7] F. J. Garcıa-Vidal, L. Martın-Moreno, *Phys. Rev. B* **2002**, *66*, 155412.

[S8] A. Taflove, S. C. Hagness, *Computational Electrodynamics: The Finite-Difference Time Domain Method*; 2nd ed., Artech, Boston, MA **2000**.

[S9] E. D. Palik, *Handbook of Optical Constants of Solids*, Academic Press, San Diego **1998**.

[S10] A. Dhawan, S. J. Norton, M. D. Gerhold, T. Vo-Dinh, *Opt. Express* **2009**, *17*, 9688.

[S11] R. S. Wagner, W. C. Ellis, *Appl. Phys. Lett.* **1964**, *4*, 89.

[S12] C.-Y. Wen, M. C. Reuter, J. Bruley, J. Tersoff, S. Kodambaka, E. A. Stach, F. M. Ross, *Science* **2009**, *326*, 1247.

[S13] M. Lynch, C. Mosher, J. Huff, S. Nettikadan, J. Johnson, E. Henderson, *Proteomics* 2004, **4**, 1695.